Negative Capacitance of an Electrolytic Cell in the Absence of Bias Potential

ARTICLE *in* THE JOURNAL OF PHYSICAL CHEMISTRY C · APRIL 2014

Impact Factor: 4.77 · DOI: 10.1021/jp412095h

2 AUTHORS:

Ioannis Lelidis

Université de Picardie Jules Verne

75 PUBLICATIONS **635** CITATIONS

SEE PROFILE

Giovanni Barbero

Politecnico di Torino

307 PUBLICATIONS **3,068** CITATIONS

SEE PROFILE

THE JOURNAL OF PHYSICAL CHEMISTRY C

Article

pubs.acs.org/JPCC

Negative Capacitance of an Electrolytic Cell in the Absence of Bias Potential

I. Lelidis*[,†,‡] and G. Barbero[†,‡]

[†]Solid State Section, Department of Physics, University of Athens, Panepistimiopolis, Zografos, Athens 157 84, Greece

[‡]Dipartimento di Scienza Applicata e Tecnologia del Politecnico di Torino, Corso Duca degli Abruzzi 24, Torino 10129, Italy

ABSTRACT: We extend the Poisson−Nernst−Planck model to the case of an electrolytic cell limited by ohmic electrodes that are partially polarizable with different affinities for anions and cations. We show that the finite conductivity of the electrodes in combination with the different ionic diffusion coefficients for anions and cations may give rise to negative capacitance behavior of the cell impedance in the absence of any bias. The range where the negative capacitance character of the electrolytic cell appears is localized. When ambipolar diffusion and electrode polarization effects are simultaneously present, the real part of the electrical impedance shows up to three plateaux.

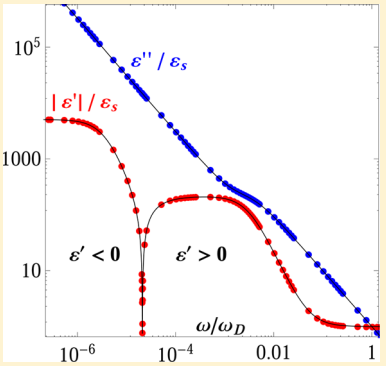

INTRODUCTION

The problem of electrode polarization (EP) is ubiquitous in impedance spectroscopy (IS), and it has mainly been modeled in the frame of the Poisson−Nernst−Planck (PNP) theory.[1−3] The PNP approach is based on the continuity equations that describe the conservation of the ions, coupled to the Poisson equation that relates the actual electrical potential with the distribution of ions in the sample. Previous investigations suggest the possibility that EP may induce negative capacitance (NC) behavior in the response of the system.[4,5] In ref 6, many experimental complex resistance plane results, which show the appearance of positive reactance (NC type), are reported. Several experimental results on impedance measurements showing the presence of NC behavior in a particular situation are also discussed in refs 7−12 and concern a large variety of materials and devices such as organic compounds, electrochemical cells, biological membranes, semiconductor devices, and so forth. Equivalent circuits have been proposed to simulate NC behavior of the system, but no continuous model has been developed. In general, materials and devices that show NC behavior are becoming quite common, but the origin of NC remains an open question.[13−15]

In the present paper, we propose a model that extends the PNP approach to the case of ohmic electrodes that have different affinity for anions and cations.[16] Our analysis is done in the continuum approximation where the ions can be considered as dimensionless point charges, the surface charge is assumed to be uniformly smeared over the surface, and the electrolytic solution is described as a continuum with uniform dielectric constant, position and time independent. As in the standard PNP model, the medium is assumed nondispersive. The frequency dependence of the effective dielectric constant is due to the presence of the ions dispersed in the solvent. In this framework, we investigate the role of EP on the IS in the presence of free and ambipolar diffusion,[17] and we demonstrate that, in the absence of a bias field, the cell can show, at low frequencies, positive reactance that can be related to NC associated to negative real part of the dielectric constant. The prerequisites for such a transition are investigated, and the state-diagram of the system is built. A similar investigation has not been reported in previous works devoted to the generalization of the PNP model.[4,5] The validity of our analysis has been tested by comparing the spectra determined by means of the presented numerical calculation with the values obtained by means of the Kramer−Kronig relations, which are valid in the linear version of the PNP model.

MODEL

Let us consider an electrolytic cell composed by an isotropic dielectric liquid between two flat electrodes parallel to the $x-y$ plane and located at $z = \pm d/2$. The electrodes are ohmic, and they exhibit different surface conductivity for cations and anions, noted as γ_p and γ_m respectively.[16] The solution contains two types of ions p, m of charge $\pm q$ and mobilities μ_p and μ_m for cations and anions, respectively. Our aim is to calculate the steady state impedance $\mathcal{Z}(\omega)$ of the cell under an applied sinusoidal voltage $V(\omega)$ of frequency $f = \omega/2\pi$ and of small enough amplitude to justify the linear treatment of the problem.[18] We do not consider the effects of generation and recombination of ions.[3,19,20] The equations that describe the system are the PNP equations:[21]

Received: December 10, 2013
Revised: March 16, 2014

   dx.doi.org/10.1021/jp412095h | J. Phys. Chem. C XXXX, XXX, XXX−XXX

$$\frac{\partial n_p}{\partial t} = -\nabla\cdot\mathbf{j}_p = D_p\nabla\cdot\left(\nabla n_p - \frac{\mu_p}{D_p}n_p\mathbf{E}\right) \quad (1)$$

$$\frac{\partial n_m}{\partial t} = -\nabla\cdot\mathbf{j}_m = D_m\nabla\cdot\left(\nabla n_m + \frac{\mu_m}{D_m}n_m\mathbf{E}\right)$$

$$\nabla\cdot\mathbf{E} = q\frac{n_p - n_m}{\varepsilon_s} \quad (2)$$

where ε_s is the dielectric permittivity of the solvent and $n_a(\mathbf{r}, t)$, with $a = p, m$, are the local densities of ions. D_a are the diffusion coefficients of the ions that are related with mobilities via the Einstein−Smoluchowski relations: $\mu_a/D_a = q/k_BT$,[22] where k_B is the Boltzmann constant and T is the temperature. The first two equations take into account the conservation of the two types of ions (equations of continuity for positive and negative ions), and the third one is the Poisson equation, relating the effective electric field $\mathbf{E}(\mathbf{r}, t)$ to the charge density.

The boundary conditions (BCs) that describe the ohmic character of the electrodes relate the ionic fluxes at the electrode−electrolyte interface with the surface conductivity of the electrodes are

$$j_a = \pm s_a E(\pm d/2, t) \quad (3)$$

where $s_a = \gamma_a/q$ and the signs ± refer to ions, that is, one has $+s_p$ and $-s_m$. According to eq 3, the current density of particles at the electrodes is proportional to the local electric field. A first use of ohmic BCs with the PNP model occurred in ref 16 for the case of ions having the same transport properties and for $\gamma_p = \gamma_m$. The particle conductivities s_a at the electrode−solution interface derive from the Butler−Volmer equation, in the limit of small overpotential[23] and are considered as constants in our framework. Other forms for the exchange current at the electrodes have been proposed in the past. According to the model of Chang−Jaffe, the conduction current at the electrodes is proportional to the variations of ionic density with respect to the value of equilibrium just in front to the electrode.[24] This form of BCs has been considered in ref 3. A possible generalization has been discussed in ref 4. The similarities and differences between the Ohmic and Chang−Jaffe models have been considered too.[5,25,26] In ref 26, the predictions of the two models relevant to the response of an electrolytic cell submitted to an ac external voltage of small amplitude are compared. In ref 26, it is proved that, by knowing the phenomenological parameter entering in one model, it is possible to determine, in a unique manner, the parameter entering in the other model, in such a manner that the electric impedance evaluated by means of the two models is the same. In general, to a real value of the Chang−Jaffe model corresponds a frequency dependent complex value of s_a. However, in the low frequency limit, where the influence of the nonblocking character of the electrodes is visible, to a real value of the Chang−Jaffe model corresponds a real value of s_a. Note that, in ref 26, the equivalence between the Ohmic model and the Chang−Jaffe one has been demonstrated in the case where only one type of ions is mobile. In our present approach, we consider both anions and cations mobile and with distinct mobilities. As it will be shown in the subsequent analysis, the latter condition is a sine qua non condition to obtain NC behavior.

Finally, the set of BCs is completed by the expression of the applied voltage at the electrodes ($z = \pm d/2$):

$$V(\pm d/2, t) = \pm(V_0/2)\exp(i\omega t) \quad (4)$$

If N is the bulk concentration of ions at thermodynamic equilibrium in the absence of external electric field, then for low enough voltage ($V \ll V_{th} = k_BT/q$), we have $n_a = N + \delta n_a(z, t)$ where $\delta n_a \ll N$ and the system can be considered as linear. The set of the PNP eq 1 and of the BCs eqs 3 and 4 after linearization is cast in the form

$$\frac{\partial p}{\partial t} = D_p\left\{\frac{\partial^2 p}{\partial z^2} - \frac{p - m}{2\lambda^2}\right\}$$

$$\frac{\partial m}{\partial t} = D_m\left\{\frac{\partial^2 m}{\partial z^2} + \frac{p - m}{2\lambda^2}\right\}$$

$$\frac{\partial^2 u}{\partial z^2} = -\frac{p - m}{2\lambda^2} \quad (5)$$

$$0 = \frac{\partial p}{\partial z} + (1 - \kappa_p)\frac{\partial u}{\partial z}$$

$$0 = \frac{\partial m}{\partial z} - (1 - \kappa_m)\frac{\partial u}{\partial z}$$

$$u(\pm d/2, t) = \pm(u_0/2)\exp(i\omega t) \quad (6)$$

where we have introduced the following reduced quantities: the reduced excess ionic density $a = \delta n_a/N$, the reduced potential $u = V/V_{th}$, and the reduced surface conductivity $\kappa_a = \gamma_a/\sigma_a$. The quantity $\sigma_a = qND_a/V_{th}$ is the bulk conductivity of the ions at thermodynamic equilibrium. $\lambda = (\varepsilon_s\ k_BT/(2Nq^2))^{1/2}$ is the Debye screening length.[22] The above linear system of second-order differential equations with constant coefficients can be solved analytically by standard methods, to determine the ionic density variation $\delta n_a(z, t)$ and the actual potential $u(z, t) = \phi(z)\exp[i\omega t]$ in the electrolytic cell that verify the associated BCs. From the BCs, it follows that the conduction across the electrodes plays an important role in the redistribution of the ionic charge only if $\kappa = \kappa_p + \kappa_m \sim 1$. If $\kappa \ll 1$, the electrodes can be considered blocking, whereas for $\kappa_a \gg 1$, they are *transparent* to the ions. The critical value for $\gamma^* = (\gamma_p + \gamma_m)^*$ separating the two regimes is then given by $\gamma^* = \sigma_p + \sigma_m$, which can be rewritten as $\gamma^*/\varepsilon_s = \omega_D$, where ω_D is the Debye relaxation frequency defined below. According to this relation, the effect of the nonblocking character of the electrodes is important when the relaxation circular frequency ω_e related to the conduction across the electrodes (defined as $\omega_e = \gamma/\varepsilon_s$) is comparable with the Debye relaxation frequency.

The current at the electrode is composed by a Faradaic and a displacement component

$$\mathcal{I} = -qS(j_p - j_m) - \varepsilon_s S\left(\frac{\partial E(z, t)}{\partial t}\right)_{d/2} \quad (7)$$

where S is the area of the electrode. Finally, the impedance of the cell is given by

$$\mathcal{Z} = \mathcal{R} + i\mathcal{X} = \frac{\mathcal{V}}{\mathcal{I}} = \frac{\phi_{(d/2)} - \phi_{(-d/2)}}{S[i\omega\varepsilon_s + (\gamma_p + \gamma_m)]\phi'_{(d/2)}} \quad (8)$$

where ϕ' is the space derivative of the electrical potential. The analytical expression of the electrical potential profile is deduced in Appendix A.

dx.doi.org/10.1021/jp412095h | J. Phys. Chem. C XXXX, XXX, XXX−XXX

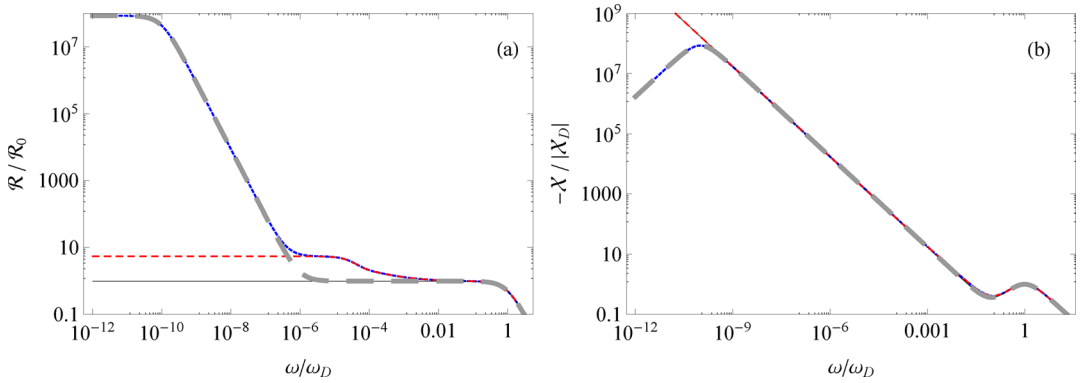

Figure 1. Plot of (a) $\mathcal{R}(\omega)/\mathcal{R}_0$, (b) $-\mathcal{X}(\omega)/|\mathcal{X}_D|$. $\mathcal{R}_0 = \mathcal{R}(0)$ for $r = 1$ and $\kappa_a = 0$; $\mathcal{X}_D = \mathcal{X}(\omega_D)$. In absence of EP ($\kappa_a = 0$) for (i) $r = 1$ thin solid line (black), (ii) $r = 0.05$ thin dashed line (red). In presence of EP, $\kappa_a = 10^{-10}$, for (iii) $r = 1$ dashed thick line (gray), (iv) $r = 0.05$ dotted line (blue). $\lambda/d = 0.0043$, $\omega_D = 3717.28$ rad s^{-1}, $\omega_{ad} = 0.123$ rad s^{-1}, $\omega_e = 3.37 \times 10^{-7}$ rad s^{-1}.

RESULTS

In the following, we analyze the frequency dependence of the electric impedance of an electrolytic cell limited by Ohmic electrodes containing one group of positive and negative ions, with different mobilities. In particular, we are interested (i) to investigate how the presence of EP and of ambipolar diffusion are manifested in the real and the imaginary part of $\mathcal{Z}(\omega)$ and (ii) to determine if the ohmic character of the electrodes could give rise to NC behavior of the cell impedance. For the numerical calculations, we consider a cell of thickness $d \gg \lambda$, and of electrode area $S = 1$ cm^2. The dielectric constant of the solvent is $\varepsilon_s = 6.7\varepsilon_0$, where ε_0 is the vacuum electrical permittivity. The bulk concentration of ions is $N = 4 \times 10^{20}$ m^{-3}, the ions are considered as monovalent, and the temperature is taken equal to $T = 300$ K. With these values for N and ε_s, we get $\lambda = 0.11$ μm. The diffusion coefficients of the ions are $D_p = 8.2 \times 10^{-11}$m^2/s and $D_m = rD_p$. The Debye or free diffusion relaxation frequency is given from $\omega_D = D_p(1 + r)/2\lambda^2$.[17] The above set of parameters corresponds to the case where the solvent is a liquid crystal.[27]

Figure 1 illustrates the real $\mathcal{R}(\omega) = \mathrm{Re}[\mathcal{Z}(\omega)]$ (a) and imaginary $\mathcal{X}(\omega) = \mathrm{Im}[\mathcal{Z}(\omega)]$ part (b) of the impedance of a cell with thickness $d = 25$ μm for some characteristic cases. The thin solid line corresponds to the case of ideally blocking electrodes (IBE) while only free diffusion is present in the cell, that is, $r = 1$. $\mathcal{R}(\omega)$ presents a plateau while $-\mathcal{X}(\omega)$ presents a local maximum at ω_D. Note that the normalization factor $\mathcal{R}_0 = \mathcal{R}(0)$ corresponds to this case ($r = 1$, $\gamma_a = 0$) and is kept the same for all curves. The dashed line refers to IBE for $r = 0.05$, that is, in presence of ambipolar diffusion. In $\mathcal{R}(\omega)$ appears now a second plateau at lower frequencies that corresponds to the ambipolar diffusion[17] with a relaxation frequency $\omega_A = (\pi/d)^2 D_A$, where $D_A = 2rD_p/(1 + r)$ is the ambipolar diffusion coefficient.[17] Ambipolar diffusion does not qualitatively change the $-\mathcal{X}(\omega)$ spectrum. When one includes the EP effect, then a new plateau appears, dotted line, in $\mathcal{R}(\omega)$ at lower frequencies than the plateau corresponding to the ambipolar diffusion ($r < 1$). For $r = 1$, dashed thick line, only two plateaux are present in $\mathcal{R}(\omega)$. As it is shown in Figure 1b, the presence of the EP effect gives rise to a second maximum in $-\mathcal{X}(\omega)$ independently from the presence or not of ambipolar diffusion. From the above analysis, one concludes that EP gives rise to a supplementary plateau in $\mathcal{R}(\omega)$ and to a second maximum in $-\mathcal{X}(\omega)$.

Figures 2 and 3 illustrate the appearance of NC behavior in the cell. The values of the model parameters are $\lambda/d = 0.0011$, $r = 0.1$, $\gamma_p = 2.1 \times 10^{-10}$ Ω^{-1} m^{-1}, and $\gamma_m = \gamma_p/20$. These values of γ_a give the reduced surface conductivities $\kappa_p = 10^{-3}$ and $\kappa_m = \kappa_p/2$. Figure 2 shows the real part $\mathcal{R}/\mathcal{R}_0$ of the impedance in reduced units versus the reduced frequency ω/ω_D, where

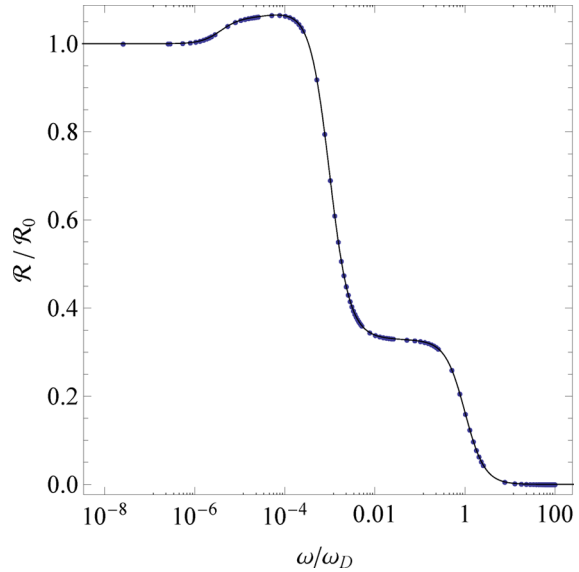

Figure 2. Semilog plot of $\mathcal{R}/\mathcal{R}_0$ vs ω/ω_D for $r = 0.1$, $\kappa_p = 10^{-3}$, and $\kappa_m = \kappa_p/2$. $\mathcal{R}(\omega)$ is not a monotonously decreasing function of ω. $\mathcal{R}(\omega)$ has a maximum at $\omega = 6.7 \times 10^{-5}$. $\omega_D = 3894.29$ rad s^{-1}. The continuous line is model calculated while the solid points are deduced by use of the Kramers–Kronig relations.

$$\mathcal{R}_0 = \frac{\lambda^2[d(\kappa_p + \kappa_m) + 2\lambda(2 - \kappa_p - \kappa_m)]}{\varepsilon_s S(D_p\kappa_p + D_m\kappa_m)} \quad (9)$$

is the resistance at zero frequency. Taking the limit of $\mathcal{Z}$ as $\kappa_a \to 0$, and after the limit of its real part for $\omega \to 0$, one retrieves its expression for blocking electrodes in presence of ambipolar diffusion $\mathcal{R}_0(\kappa_a = 0) = \lambda^2 d/(\varepsilon S D_A)$[17] that further reduces to $\mathcal{R}_0 = \lambda^2 d/\varepsilon_s SD$, when $D_p = D_m = D$. Note that, in the dc limit, the reactance of the cell vanishes. This means that, in this limit,

dx.doi.org/10.1021/jp412095h | J. Phys. Chem. C XXXX, XXX, XXX−XXX

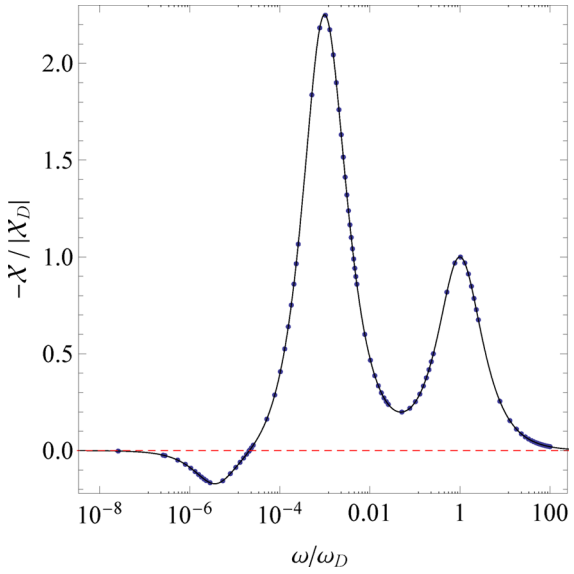

Figure 3. Semilog plot of $-\mathcal{X}/|\mathcal{X}_D|$ vs ω/ω_D for the same parameters as in Figure 2. $\mathcal{X}_D = \mathcal{X}(\omega_D)$. $\mathcal{X}(\omega)$ presents a change of sign at $\omega_c/\omega_D = 2.1 \times 10^{-5}$ that signifies the appearance of NC at lower frequencies than ω_c. The horizontal dashed red line is the zero level line, $\mathcal{X} = 0$. The continuous line is model calculated while the solid points are deduced by use of the Kramers–Kronig relations.

the cell behaves as a true resistance whose value is $\mathcal{R}_0$, as expected, because the electrodes are nonblocking. Since $\lim_{\omega\to 0} \mathcal{X} = 0$, in the dc limit, the behavior of the cell is of inductive type.

As it is shown in Figure 2, the resistance is a nonmonotonic function of the frequency, and it presents a large peak centered at $\omega/\omega_D = 6.7 \times 10^{-5}$. This nonmonotonic behavior of $\mathcal{R}$ is a signature of inductive behavior that is of course a nongenuine induction, since it appears only at low frequency. For a genuine inductive behavior, the NC should appear at "high" frequencies.[14] In Figure 3, $-\mathcal{X}(\omega)$ shows three extrema. The maximum at the higher frequency corresponds to ω_D. The second maximum appears at the frequency $\omega/\omega_D = 9.5 \times 10^{-4}$ that is related to ω_c. At lower frequency, the dependence of $-\mathcal{X}$ on ω becomes steeper than the -1 power, and the sign of $\mathcal{X}$ changes, indicating the appearance of NC. The frequency ω_c where $\mathcal{X}(\omega_c) = 0$ moves to higher values when the concentration of ions is increasing. The last extremum is a minimum, and it appears in the NC range. Its position corresponds to the ambipolar diffusion relaxation frequency $\omega_A/\omega_D = 3.8 \times 10^{-6}$.

Figure 4 gives the complex plane response (Cole–Cole diagram) of the cell. The NC appears at low frequencies as a negative semicircle that corresponds to a positive reactance. In order to preserve the usual semicircular aspect of the parametric plot, we do not use reduced units in Figure 4.

In some cases, it is useful to perform the analysis of the impedance spectroscopy data at the dielectric level, where the real, ε', and imaginary, ε'', parts of the complex dielectric constant $\varepsilon = \varepsilon' - i\varepsilon''$ are determined. In this framework, the calculation of the complex impedance is done by introducing the complex capacitance $C = \varepsilon(S/d)$. It follows that the impedance of the cell is given by $\mathcal{Z} = 1/(i\omega C)$. By separating the real and imaginary parts, we get

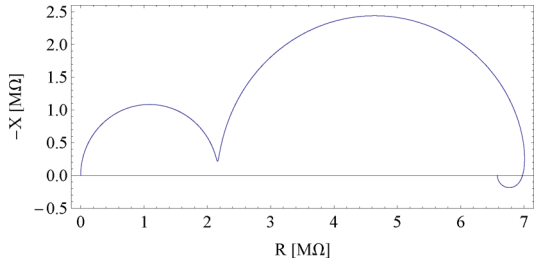

Figure 4. Nyquist diagram of the electrolytic cell calculated for the same conditions as in Figure 2.

$$\mathcal{R} = \frac{\varepsilon''}{\omega(\varepsilon'^2 + \varepsilon''^2)}\frac{d}{S} \quad \text{and} \quad \mathcal{X} = -\frac{\varepsilon'}{\omega(\varepsilon'^2 + \varepsilon''^2)}\frac{d}{S} \tag{10}$$

from which it follows that

$$\varepsilon' = -\frac{\mathcal{X}}{\omega(\mathcal{R}^2 + \mathcal{X}^2)}\frac{d}{S} \quad \text{and} \quad \varepsilon'' = \frac{\mathcal{R}}{\omega(\mathcal{R}^2 + \mathcal{X}^2)}\frac{d}{S} \tag{11}$$

Figure 5a shows the real part of the reduced dielectric function $\varepsilon'(\omega)/\varepsilon_s$ versus the reduced frequency. At frequencies lower than the cusp frequency ω_c, the system shows NC and $\varepsilon'(\omega) < 0$. ω_c is displaced to higher values as κ increases. The loss $\varepsilon''(\omega)$ follows the power law ω^{-1} in frequency (Figure 5b).

In some other cases, the analysis is performed at the conductivity level, where the real, σ', and imaginary, σ'', parts of the complex conductivity $\sigma = \sigma' + \sigma''$ are measured. In this framework, the calculation of the complex impedance is done by means of the complex resistance $\mathcal{Z} = R = (1/\sigma)(d/S)$. By separating again the real and imaginary parts, we get

$$\mathcal{R} = \frac{\sigma'}{\sigma'^2 + \sigma''^2}\frac{d}{S} \quad \text{and} \quad \mathcal{X} = -\frac{\sigma''}{\sigma'^2 + \sigma''^2}\frac{d}{S} \tag{12}$$

from which we obtain

$$\sigma' = \frac{\mathcal{R}}{\mathcal{R}^2 + \mathcal{X}^2}\frac{d}{S} \quad \text{and} \quad \sigma'' = -\frac{\mathcal{X}}{\mathcal{R}^2 + \mathcal{X}^2}\frac{d}{S} \tag{13}$$

From eq 11, it follows that, for $\mathcal{X} < 0$, $\varepsilon' > 0$ and $\varepsilon'' > 0$, whereas for $\mathcal{X} > 0$, $\varepsilon' < 0$ and $\varepsilon'' > 0$. A similar analysis at the conductivity level indicates that, for $\mathcal{X} < 0$, $\sigma' > 0$ and $\sigma'' > 0$, and for $\mathcal{X} > 0$, $\sigma' > 0$ and $\sigma'' < 0$. In Figure 6, we show the real σ' and imaginary σ'' parts of the conductivity function $\sigma = \sigma' + i\sigma''$ calculated under the same conditions as in Figure 2. σ'' becomes negative at frequencies lower than ω_c. In the high frequency limit ($\omega \to \infty$), the real part of the conductivity σ' tends to $\sigma_\infty = \varepsilon_s\omega_D$.

In the dc limit, $\lim_{\omega\to 0} \varepsilon' = -\mathcal{X}_1 d/S\mathcal{R}_0^2$, where $\mathcal{X}_1$ is the coefficient of the leading term in the low frequency expansion of $\mathcal{X} = \mathcal{X}_1\omega + O(1)$. At low frequency, $\varepsilon'' \sim (d/S\mathcal{R}_0)\omega^{-1}$, and therefore, as $\omega \to 0$, ε'' diverges. Since now $\sigma' = \varepsilon''\omega$ and $\sigma'' = \varepsilon'\omega$, one finds in the dc limit for the complex conductivity $\lim_{\omega\to 0} \sigma' = d/S\mathcal{R}_0$ and $\lim_{\omega\to 0} \sigma'' = 0$.

Figure 7 presents the state-diagram in the plane r–κ_p for $\kappa_m = 0.5\kappa_p$. The region of NC behavior of the electrolytic cell is indicated in gray (yellow on line). Outside this region $\mathcal{R}$ is a monotonic function of ω with negative slope.

Finally, note that, when anions and cations have the same mobility ($r = 1$), that is, in absence of the ambipolar effect, the system never presents a NC regime. On the contrary, different surface conductivities is not a necessary condition to observe a

dx.doi.org/10.1021/jp412095h | J. Phys. Chem. C XXXX, XXX, XXX–XXX

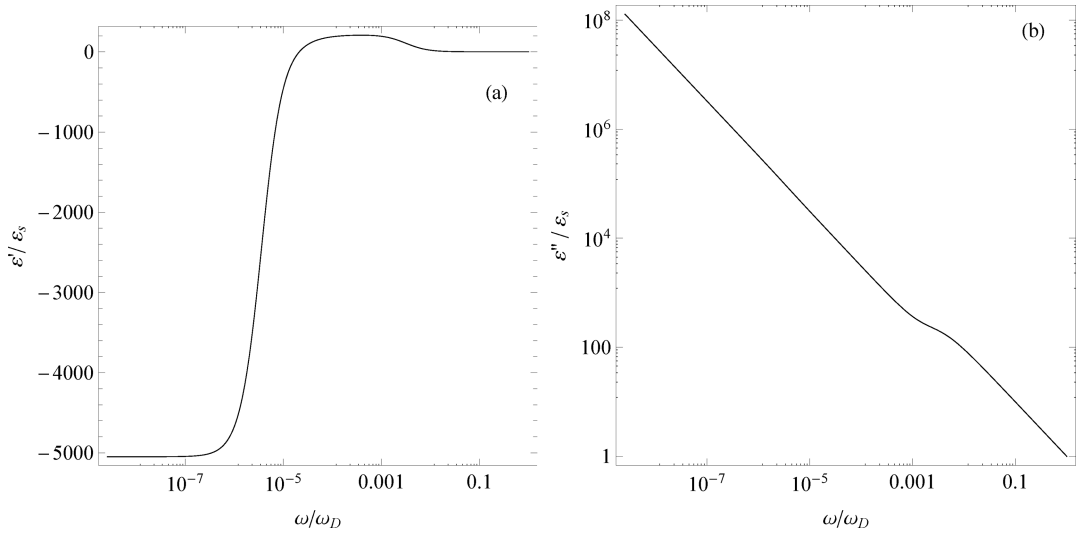

Figure 5. Semilog plot of the real (a) and log–log plot of the imaginary (b) part of the dielectric function $\varepsilon = \varepsilon' - i\varepsilon''$ calculated under the same conditions as in Figure 2. $\varepsilon'(\omega)$ is negative at frequencies lower than the ω_c frequency.

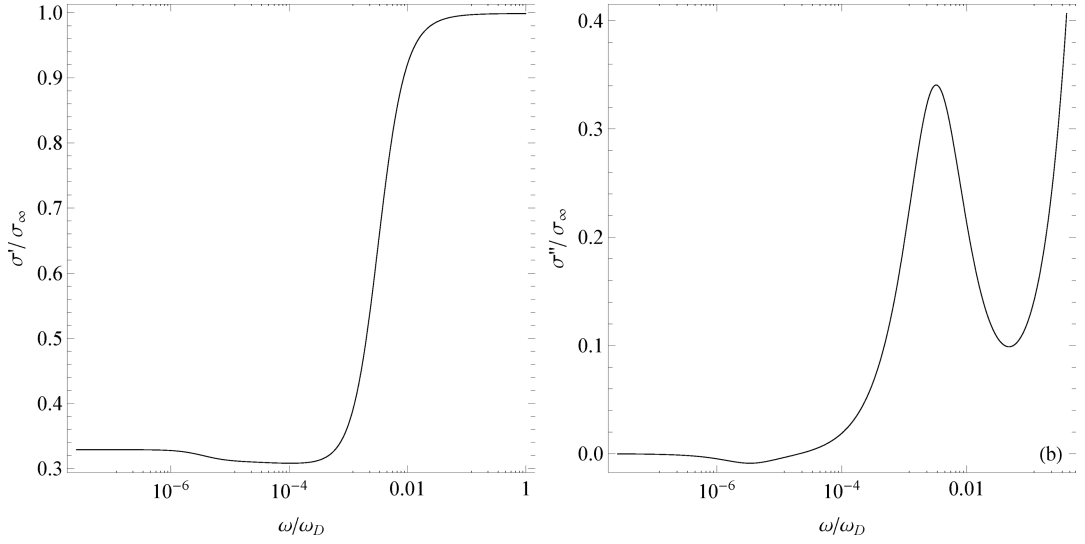

Figure 6. Semilog plot of the real (a) and imaginary (b) part of the conductivity function $\sigma = \sigma' + i\sigma''$ calculated under the same conditions as in Figure 2. σ'' becomes negative at frequencies lower than the ω_c frequency. $\sigma_\infty = \varepsilon_s\omega_D$.

NC regime. Therefore, it seems that the physical mechanism responsible for NC behavior originates from a coupling between the ambipolar diffusion that is a volume effect and the EP that is a surface effect.

KRAMERS–KRONIG RELATIONS

Since our physical system is governed by eq 5 with the boundary conditions eq 6 that are all linear differential equations with constant coefficient, one expects that the real, $\mathcal{R}$, and imaginary, $\mathcal{X}$, parts of $\mathcal{Z}$ have to verify the Kramers–Kronig (KK) relations.[28] For the system under consideration, the KK relations are

$$\mathcal{R}(\omega) = -\frac{2}{\pi}\mathcal{P}\int_0^\infty \frac{\omega'\mathcal{X}(\omega')}{\omega'^2 - \omega^2}\mathrm{d}\omega' \tag{14}$$

$$\mathcal{X}(\omega) = -2\frac{\omega}{\pi}\mathcal{P}\int_0^\infty \frac{\mathcal{R}(\omega') - \varepsilon_s}{\omega'^2 - \omega^2}\mathrm{d}\omega' \tag{15}$$

where $\mathcal{P}$ means the principal part of the integral, on the real axis. Equations 14 and 15 coincide with eqs 22.58 and 22.57 reported in Chapter 22 of ref 28, respectively. To test the validity of the numerical analysis presented above, in Figures 2 and 3, we compare the spectra of $\mathcal{R}$ and $\mathcal{X}$ derived by means of eq 8 with the values (solid points) derived by the KK relations eqs 14 and15. The agreement is perfect, validating the results of the presented numerical calculation. This agreement has been verified with different sets of numerical parameters (not shown in the paper).

By operating in a standard manner, it is possible to write KK relations at the dielectric level. They take the form[29]

$$\varepsilon'(\omega) - \varepsilon_s = \frac{2}{\pi}\mathcal{P}\int_0^\infty \frac{\omega'\varepsilon''(\omega')}{\omega'^2 - \omega^2}\mathrm{d}\omega' \tag{16}$$

$$\varepsilon''(\omega) = -2\frac{\omega}{\pi}\mathcal{P}\int_0^\infty \frac{\varepsilon'(\omega') - \varepsilon_s}{\omega'^2 - \omega^2}\mathrm{d}\omega' \tag{17}$$

dx.doi.org/10.1021/jp412095h | J. Phys. Chem. C XXXX, XXX, XXX–XXX

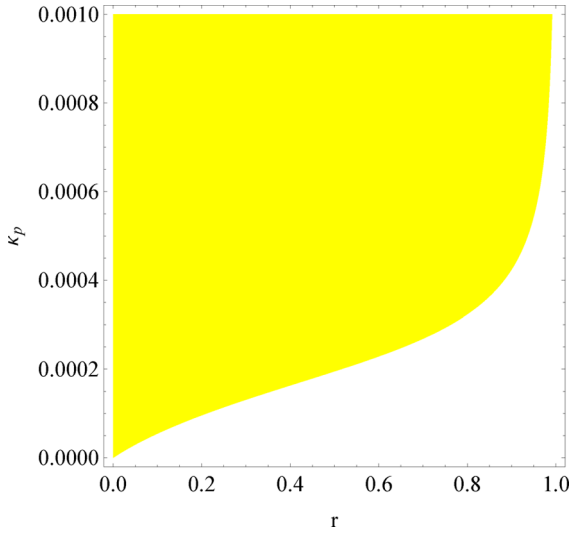

Figure 7. State-diagram of an electrolytic cell in the $r-\kappa_p$ plane with $\lambda/d = 0.0011$ and $\kappa_m/\kappa_p = 0.5$. Inside the filled region the capacitance of the cell is negative while it becomes positive outside.

In Figure 8, we compare the spectra of ε' and ε'' evaluated by means of eq 11 with the values of the same quantity determined by means of eqs 16 and 17. The agreement is perfect again, as expected.

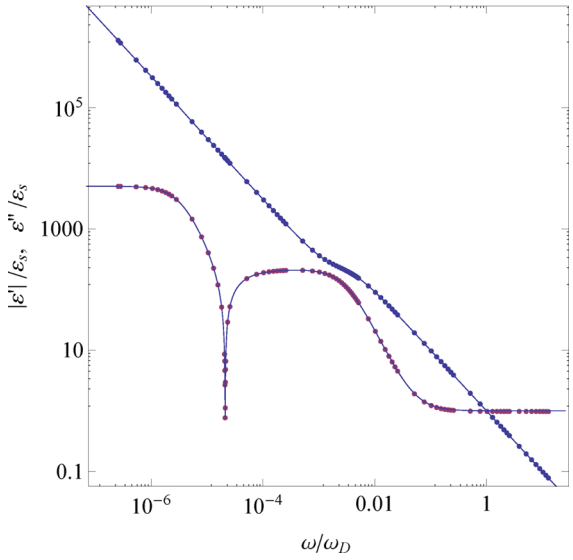

Figure 8. Absolute value of the real $\varepsilon'(\omega)$ part and the imaginary $\varepsilon''(\omega)$ part of the dielectric constant calculated from the Kramers–Kronig relations (solid points). Continuous lines are produced by the model. ε' shows a cusp at a frequency ω_c below which $\varepsilon' < 0$.

CONCLUSION

We extended the PNP model to treat the case of a cell with ohmic electrodes when charge exchange is present. The surface conductivity of the electrodes and the ionic diffusivity are assumed different for anions and cations. We localized a domain in the parameter space of the problem where the system exhibits a negative capacitance which results to a nonmonotonic variation of the cell resistance that appears as an oscillation or a peak. This "anomaly" may be of low amplitude in $\mathcal{R}$, but it gives rise to a singular behavior in the $|\mathcal{X}|$ part of the impedance where it appears a cusp, that is, $\mathcal{X}$ changes its sign at some frequency. Our results retrieve experimental observations of negative capacitance in electrolytic cells that up to now were described with equivalent circuit theory. We have tested that the real, $\mathcal{R}$, and imaginary, $\mathcal{X}$, parts of the numerically calculated spectra of $\mathcal{Z}$ verify the Kramers–Kronig relations, as they should in the linear version of the PNP model. Finally, we note that typically negative capacitance behavior arises in the presence of a dc bias,[7,8,10,13], but our model shows that such a dc bias is not strictly necessary. The dependence of the negative capacitance response on the ohmic parameters values is under investigation. The present work could be extended to include other effects such as generation–recombination of ions that can add in the $\mathcal{R}(\omega)$ another plateau,[20] adsorption and diffusion bottleneck of ions at the electrodes, asymmetric in nature electrodes, and so forth.

In our analysis, we have assumed that the ohmic boundary condition parameters are real for the mobile charges of each sign. But it is well known that PNP analyses with real reaction rates of Chang–Jaffe type,[24] the approach primarily used in the past for successful analyses of the electrical response of a variety of different materials, do not lead to any negative capacitative effects. It is only when these parameters are generalized to become complex that such effects appear and are then identified as being associated with specific adsorption at the electrodes.[3] As discussed in ref 26, the Chang–Jaffe and Ohmic models are completely equivalent for the one mobile group approximation, in the sense that to a real phenomenological parameter of a model corresponds a real phenomenological parameter of the other model. Suppose it is possible to prove that the Chang–Jaffe and Ohmic models are equivalent also in the case where both ions are mobile because, in the linear limit, the bulk differential equations in the two models are the same, as discussed above. In addition, they contain the same number of integration constants for what concerns the reduced potential and ionic densities. By substituting these expressions in the boundary conditions, assume it is possible to transform the ones of one model in those of the other model, by choosing the phenomenological parameter in a proper manner. However, even in this case, to a real value of the phenomenological parameter of one model corresponds a complex parameter of the other model. Although in our analysis the negative capacitance effects are not identified with specific adsorption, they may be of this character for the correspondence between real and complex phenomenological parameters of the two models, and we will discuss this possibility elsewhere.

APPENDIX A: ANALYTICAL SOLUTION

In this appendix, we solve analytically the fundamental eq 5 of the problem with the BCs eq 6. Since the aforementioned system of differential equations has constant coefficients, the solutions are of the type

$$p(z, t) = R_p(z)\exp(i\omega t) \tag{18}$$

$$m(z, t) = R_m(z)\exp(i\omega t) \tag{19}$$

$$u(z, t) = \phi(z)\exp(i\omega t) \tag{20}$$

The substitution of the above trial solutions into eqs 5 and 6 gives

dx.doi.org/10.1021/jp412095h | J. Phys. Chem. C XXXX, XXX, XXX–XXX

$$R''_p(z) - \frac{1}{l_p^2}R_p(z) + \frac{1}{2\lambda^2}R_m(z) = 0$$

$$R''_m(z) - \frac{1}{l_m^2}R_m(z) + \frac{1}{2\lambda^2}R_p(z) = 0$$

$$\phi''(z) = -\frac{1}{2\lambda^2}[R_p(z) - R_m(z)] \quad (21)$$

and

$$R'_p + (1-\kappa_p)\phi' = 0$$

$$R'_m - (1-\kappa_m)\phi' = 0$$

$$\phi(\pm d/2) = \pm u_0/2 \quad (22)$$

where the prime means derivation with respect to z and

$$\frac{1}{l_p^2} = \frac{1}{2\lambda^2}\left(1 + 2i\omega\frac{\lambda^2}{D_p}\right)$$

$$\frac{1}{l_m^2} = \frac{1}{2\lambda^2}\left(1 + 2i\omega\frac{\lambda^2}{D_m}\right) \quad (23)$$

After some algebra, the functions $R_p(z)$, $R_m(z)$, and $\phi(z)$, solutions of eq 21 with the BCs eq 22 are calculated:

$$R_p(z) = C_1^p e^{\nu_1 z} + C_2^p e^{-\nu_1 z} + C_3^p e^{\nu_2 z} + C_4^p e^{-\nu_2 z}$$

$$R_m(z) = k_1(C_1^p e^{\nu_1 z} + C_2^p e^{-\nu_1 z}) + k_2(C_3^p e^{\nu_2 z} + C_4^p e^{-\nu_2 z})$$

$$\phi(z) = -\frac{1}{2\lambda^2}\left[\frac{1-k_1}{\nu_1^2}(C_1^p e^{\nu_1 z} + C_2^p e^{-\nu_1 z}) + \frac{1-k_2}{\nu_2^2}(C_3^p e^{\nu_2 z} + C_4^p e^{-\nu_2 z})\right] + Az + B \quad (24)$$

where

$$k_{1,2} = -2\lambda^2\left(\nu_{1,2}^2 - \frac{1}{l_p^2}\right)$$

and

$$\nu_{1,2} = \frac{1}{\sqrt{2}\lambda}\sqrt{1 + i\omega\lambda^2\frac{D_p + D_m}{D_p D_m} \pm \sqrt{1 + \left(i\omega\lambda^2\frac{D_m - D_p}{D_m D_p}\right)^2}}$$

The integration constants A, B, and C_j^a, where $j = 1, 2, 3, 4$ and $a = p, m$, are determined by the BCs eq 22, and finally the solutions may be cast in the form

$$R_p(z) = 2C_1^p\sinh(\nu_1 z) + 2C_3^p\sinh(\nu_2 z)$$

$$R_m(z) = 2k_1C_1^p\sinh(\nu_1 z) + 2k_2C_3^p\sinh(\nu_2 z)$$

$$\phi(z) = \frac{k_1 - 1}{\nu_1^2\lambda^2}C_1^p\sinh(\nu_1 z) + \frac{k_2 - 1}{\nu_2^2\lambda^2}C_3^p\sinh(\nu_2 z) + Az \quad (25)$$

where

$$A = \frac{u_0}{d} + \frac{2}{d\lambda^2}\left[\frac{1-k_1}{\nu_1^2}C_1^p\sinh(\nu_1 d/2) + \frac{1-k_2}{\nu_2^2}C_3^p\sinh(\nu_2 d/2)\right] \quad (26)$$

$$C_1^p = \{[\Gamma_4(1-\kappa_p) + \Gamma_2(1-\kappa_m)]\nu_1^2\nu_2^2u_0\lambda^2C_2\}/\{2C_1S_2(-1+k_2)[\Gamma_3(\kappa_p-1) + \Gamma_1(\kappa_m-1)]\nu_1^2 + 2C_2S_1\nu_2^2(-1+k_1)[\Gamma_4(1-\kappa_p) + \Gamma_2(1-\kappa_m)] - 2C_2C_1d\lambda^2\nu_1^2\nu_2^2(\Gamma_1\Gamma_4 - \Gamma_2\Gamma_3)\} \quad (27)$$

$$C_3^p = \{-[\Gamma_3(1-\kappa_p) + \Gamma_1(1-\kappa_m)]\nu_1^2\nu_2^2u_0\lambda^2C_1\}/\{2C_1S_2(-1+k_2)[\Gamma_3(\kappa_p-1) + \Gamma_1(\kappa_m-1)]\nu_1^2 + 2C_2S_1\nu_2^2(-1+k_1)[\Gamma_4(1-\kappa_p) + \Gamma_2(1-\kappa_m)] - 2C_2C_1d\lambda^2\nu_1^2\nu_2^2(\Gamma_1\Gamma_4 - \Gamma_2\Gamma_3)\} \quad (28)$$

with

$$\Gamma_1 = \nu_1 - \frac{1-k_1}{2\lambda^2\nu_1}(1-\kappa_p)$$

$$\Gamma_2 = \nu_2 - \frac{1-k_2}{2\lambda^2\nu_2}(1-\kappa_p)$$

$$\Gamma_3 = \nu_1k_1 + \frac{1-k_1}{2\lambda^2\nu_1}(1-\kappa_m)$$

$$\Gamma_4 = \nu_2k_2 + \frac{1-k_2}{2\lambda^2\nu_2}(1-\kappa_m)$$

and

$$C_i = \cosh\left(\frac{d}{2}\nu_i\right) \quad S_i = \sinh\left(\frac{d}{2}\nu_i\right) \quad \text{with} \quad i = 1, 2$$

AUTHOR INFORMATION

Corresponding Author

*E-mail: ilelidis@phys.uoa.gr.

Notes

The authors declare no competing financial interest.

ACKNOWLEDGMENTS

We acknowledge financial support from the Thales Grant of the Hellenic Ministry of Education.

REFERENCES

(1) Macdonald, J. R.; Johnson, W. B. Fundamentals of Impedance Spectroscopy. *Impedance Spectroscopy: Theory, Experiment, and Applications*; Barsoukov, E., Macdonald, J. R., Eds., Wiley & Sons: New York, 2005; pp 1−26.

(2) Macdonald, J. R. Theory of ac Space-Charge Polarization Effects in Photoconductors, Semiconductors, and Electrolytes. *Phys. Rev.* **1953**, *92*, 4−17.

(3) Macdonald, J. R.; Franceschetti, D. R. Theory of Small-Signal ac Responce of Solids and Liquids with Recombining Mobile Charge. *J. Chem. Phys.* **1978**, *68*, 1614−1637.

(4) Franceschetti, D. R.; Macdonald, J. R. Electrode Kinetics, Equivalent Circuits, and System Characterization: Small-Signal Conditions. *J. Electroanal. Chem.* **1977**, *82*, 271−301.
(5) Macdonald, J. R. Utility and Importance of Poisson−Nernst−Planck Immittance-Spectroscopy Fitting Models. *J. Phys. Chem. C* **2013**, *117*, 23433−23450.
(6) Macdonald, D. D.; McKubre, M. C. H. Corrosion of Materials. *Impedance Spectroscopy: Theory, Experiment, and Applications*; Barsoukov, E., Macdonald, J. R., Eds.; Wiley & Sons: New York, 2005; pp 343−429.
(7) Ciureanu, M.; Wang, H.; Qi, Z. Electrochemical Impedance Study of Membrane-Electrode Assemblies in PEM Fuel Cells. II. Electrooxidation of H_2 And H_2/Co Mixtures on Pt/Ru-Based Gas-Diffusion Electrodes. *J. Phys. Chem. B* **1999**, *103*, 9645−9657.
(8) Hens, Z.; Gomes, W. P. Photoanodic Dissolution of n-InP: An Electrochemical Impedance Study. *J. Phys. Chem. B* **2000**, *104*, 7725−7734.
(9) Sanabria, H.; Miller, J. H. Relaxation Processes Due to the Electrode-Electrolyte Inter face in Ionic Solutions. *Phys. Rev.* **2006**, *74*, 051505−1−9.
(10) Mora-Seró, I.; Bisquert, J.; Fabregat-Santiago, F.; Garcia-Belmonte, G.; Zoppi, G.; Durose, K.; Proskuryakov, Y. Y.; Oja, I.; Belaidi, A.; Dittrich, T.; et al. Implications of the Negative Capacitance Observed at Forward Bias in Nanocomposite and Polycrystalline Solar Cells. *Nano Lett.* **2006**, *6*, 640−650.
(11) Bisquert, J. A Variable Series Resistance Mechanism to Explain the Negative Capacitance Observed in Impedance Spectroscopy Measurements of Nanostructured Solar Cells. *Phys. Chem. Chem. Phys.* **2011**, *13*, 4679−4685.
(12) Bolzán, A. E.; Gassa, L. M. Comparative EIS Study of the Adsorption and Electro-oxidation of Thiourea and Tetramethylthiourea on Gold Electrodes. *J. Appl. Electrochem.* **2014**, *44*, 279−292.
(13) Shulman, J.; Tsui, S.; Chen, F.; Xue, Y. Y.; Chu, C. W. Plasmalike Negative Capacitance in Nanocolloids. *Appl. Phys. Lett.* **2007**, *90*, 032902−1−3.
(14) Johnscher, A. K. The Physical Origin of Negative Capacitance. *J. Chem. Soc. Faraday Trans. 2* **1986**, *82*, 75−81.
(15) Ramakrishna, S. A. Physics of Negative Refractive Index Materials. *Rep. Prog. Phys.* **2005**, *68*, 449−521.
(16) Barbero, G.; Batalioto, P.; Figueiredo Neto, A. M. Impedance Spectroscopy of an Electrolytic Cell Limited by Ohmic Electrodes. *J. Appl. Phys.* **2007**, *101*, 054102−1−5.
(17) Barbero, G.; Lelidis, I. Evidence of the Ambipolar Diffusion in the Impedance Spectroscopy of an Electrolytic Cell. *Phys. Rev. E* **2007**, *76*, 051501−1−9.
(18) Barbero, G.; Alexe-Ionescu, A. L.; Lelidis, I. Significance of Small Voltage in Impedance Spectroscopy Measurements on Electrolytic Cells. *J. Appl. Phys.* **2005**, *98*, 113703−1−5.
(19) Barbero, G.; Lelidis, I. Electrical Response of a Medium Containing Dissociable Impurities. *J. Phys. Chem. B* **2011**, *115*, 3496−3504.
(20) Lelidis, I.; Barbero, G.; Sfarna, A. Comparison of Two Generation-Recombination Terms in the Poisson-Nernst-Planck Model. *J. Chem. Phys.* **2012**, *137*, 154104−1−10.
(21) Bazant, M. Z.; Thornton, K.; Ajadari, A. Diffuse-Charge Dynamics in Electrochemical Systems. *Phys. Rev. E* **2004**, *70*, 021506−1−24.
(22) Atkins, P. W. *Physical Chemistry*; Oxford University Press: Oxford, U.K., 2000.
(23) Van Soestbergen, M. Frumkin−Butler−Volmer Theory and Mass Transfer in Electro chemical Cells. *Russ. J. Electrochem.* **2012**, *48*, 570−579.
(24) Chang, H.; Jaffe, G. Polarization in Electrolytic Solutions. Part I. Theory. *J. Chem. Phys.* **1952**, *20*, 1071−1077.
(25) Macdonald, J. R. Effects of Various Boundary Conditions on the Response of Poisson-Nernst-Planck Impedance Spectroscopy Analysis Models and Comparison with a Continuous-Time Random-Walk Model. *J. Phys. Chem. A* **2011**, *115*, 13370−13380.
(26) Barbero, G.; Scalerandi, M. Similarities and Differences among the Models Proposed for Real Electrodes in the Poisson-Nernst-Planck Theory. *J. Chem. Phys.* **2012**, *136*, 084705−1−7.
(27) Sawada, A.; Tarumi, K.; Naemura, S. Effects of Electric Double Layer and Space Charge Polarization by Plural Kinds of Ions on Complex Dielectric Constant of Liquid Crystal Materials. *Jpn. J. Appl. Phys. Part I* **1999**, *38*, 1418−1422.
(28) Orazem, M. E.; Tribollet, B. *Electrochemical Impedance Spectroscopy*; John Wiley: Hoboken, NJ, 2008.
(29) Landau, L.; Lifchitz, E. *Physique Theorique: Electrodynamique des Milieux Continus*; MIR: Moscow, Russia, 1990.